Nuclear Engineering and Technology 48 (2016) 1219–1229

Available online at ScienceDirect

Nuclear Engineering and Technology

journal homepage: www.elsevier.com/locate/net

Original Article

Computer Modeling, Characterization, and Applications of Gallium Arsenide Gunn Diodes in Radiation Environments

Wafaa Abd El-Basit [a,*], *Safaa Mohamed El-Ghanam* [a], *Ashraf Mosleh Abdel-Maksood* [b], *Sanaa Abd El-Tawab Kamh* [a], *and Fouad Abd El-Moniem Saad Soliman* [b]

[a] *Electronics Research Laboratory, Physics Department, Faculty of Women for Arts, Science and Education, Ain-Shams University, Heliopolis, Cairo, Egypt*

[b] *Nuclear Materials Authority, P.O. Box 530, Maadi, 11728, Cairo, Egypt*

ARTICLE INFO

Article history:
Received 25 January 2016
Received in revised form
30 March 2016
Accepted 19 April 2016
Available online 24 May 2016

Keywords:
Domain Excess Field
Gamma Dose
Microwave Oscillator
Mobility
Neutron Fluence
Shelf Annealing
Transferred Electron Devices

ABSTRACT

The present paper reports on a trial to shed further light on the characterization, applications, and operation of radar speed guns or Gunn diodes on different radiation environments of neutron or γ fields. To this end, theoretical and experimental investigations of microwave oscillating system for outer-space applications were carried out. Radiation effects on the transient parameters and electrical properties of the proposed devices have been studied in detail with the application of computer programming. Also, the oscillation parameters, power characteristics, and bias current were plotted under the influence of different γ and neutron irradiation levels. Finally, shelf or oven annealing processes were shown to be satisfactory techniques to recover the initial characteristics of the irradiated devices.

1. Introduction

The electrical properties of semiconductor devices are greatly influenced by irradiation, i.e., both the forward- and reverse-electrical (I–V) characteristic curves are changed. However, the magnitude of those changes depends on the type of semiconductor, on the design of the device and on the operating conditions. Accordingly, the radiation stability of diodes is sometimes determined by the degree of deformation of the forward (I–V) characteristics and sometimes by the changes in reverse characteristics [1–5]. Transferred electron devices (TEDs), sometimes called Gunn diodes,

* *Corresponding author.*
E-mail address: wafaa.abdelbasit@women.asu.edu.eg (W. Abd El-Basit).
http://dx.doi.org/10.1016/j.net.2016.04.009

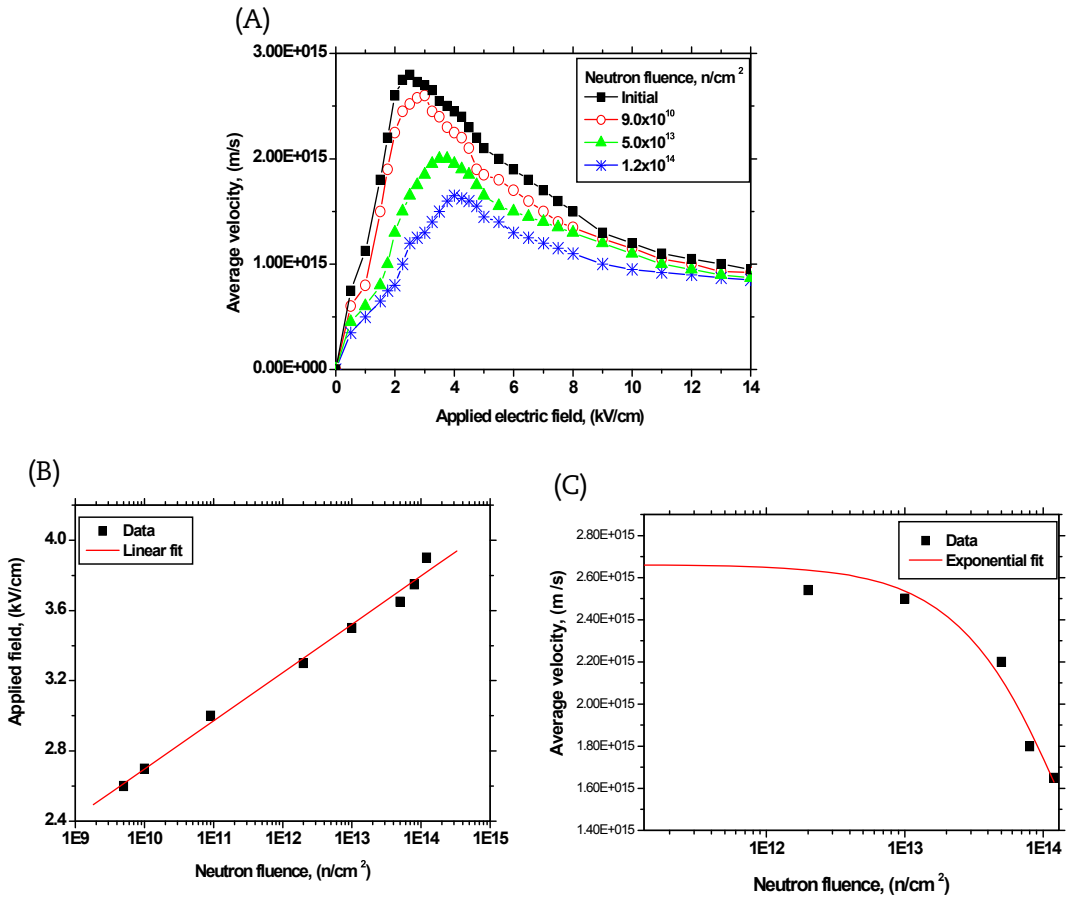

Fig. 1 – Average velocities. Calculated average velocity as a function of (A) applied electric field and (B) applied field. (C) Average velocity as a function of neutron fluence.

have been a topic for active research since 1965 [6,7]. The Gunn diode is a unique component. Even though it is called a diode, it does not contain a positive–negative diode junction. The Gunn diode can be termed a diode because it has two electrodes. It depends upon the bulk material properties rather than that of a positive–negative junction. The Gunn diode operation depends on the fact that it has a voltage-controlled negative resistance [8]. A possible application of these diodes involves satellites and military communications where radiation tolerance is desired. Damage in GaAs devices results from the displacement of lattice atoms and their subsequent migration and trapping to form stable and metastable defects. These defects lead to a pronounced change in both the static and dynamic characteristics, but not necessarily in the same way. In addition, different defects may arise from various radiation types, flux rates, and energies.

The principal effect of high energy neutrons on GaAs is to produce defect clusters, which act as trapping and scattering centers for free carriers. In turn, the effect of these clusters on the device characteristics can be modeled by a carrier removal rate and a fluence-dependent effective mobility describing the decrease in carrier mobility and the reduction in the effective carrier concentration.

2. Materials and methods

2.1. Computer modeling

To study the radiation effects on the output characteristics of the transferred electron device, a computer model has been developed (by the authors) in order to solve the transient characteristics of the diode such as charge carrier mobility, domain excess potential, and the outside domain electric field. In addition, the waveforms of current density value as a function of time for the oscillating diode were obtained under the influence of different neutron fluence (φ) levels. All the analyses of the domain behavior of GaAs devices are based on its velocity–field (υ-E) characteristics [8–13]. Among them, the Thim [8] model was chosen to be used for this study, where:

$$\upsilon = \upsilon(E) = \left[\mu_1 \cdot E + \upsilon_V \cdot (E/E_o)^4\right] \cdot \left[1 + (E/E_o)^4\right]^{-1} \quad (1)$$

where υ: velocity; μ_1: measure of how quickly an electron can move through a metal or semiconductor; = 8,000 $cm^2/V.s$; E: applied field in kV/cm; υ_v: valley velocity and $E_o = 4.0$ kV/cm.

For current calculations, one considers a uniformly doped GaAs diode to which an electric field is applied, which biases it to the negative differential mobility region. Any disturbance in the field will grow and thus produce a high field domain. In the

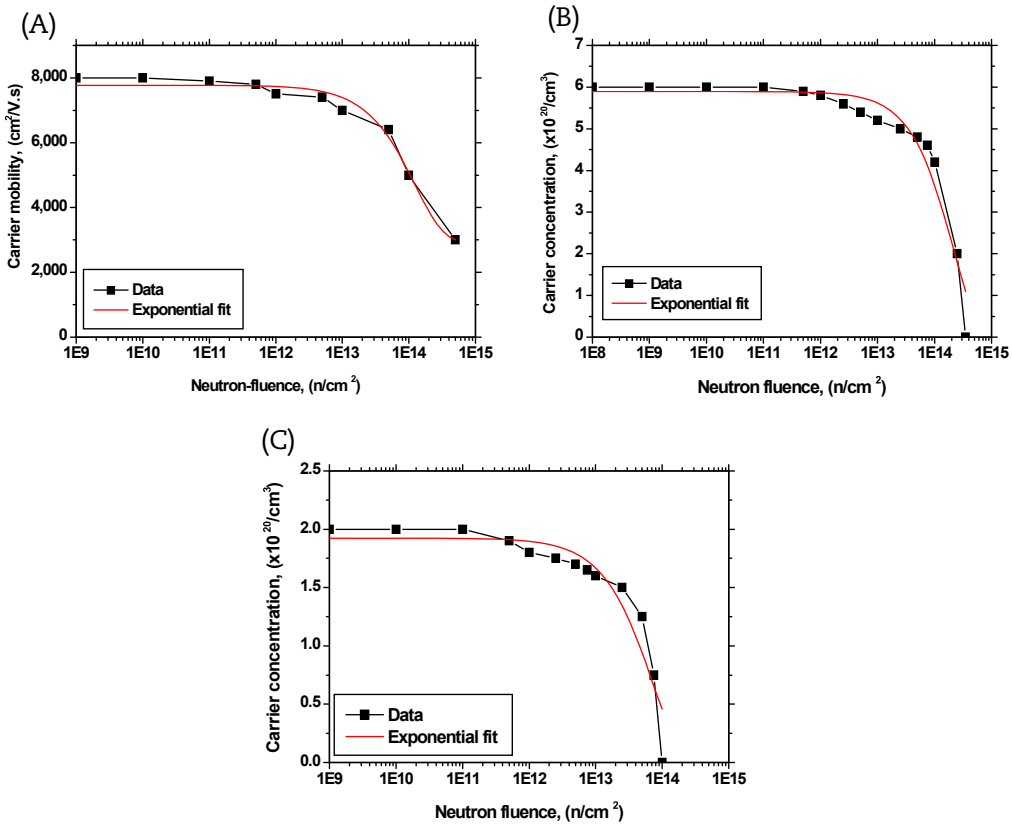

Fig. 2 – Calculated mobility and concentration. (A) Calculated mobility. Calculated concentration for (B) electrons and (C) holes as a functions of neutron fluence.

low field region, the total current will be due to conduction current and displacement current in this region, while the field $E_o(t)$ does not vary in the longitudinal direction. This implies that the charge density is uniform and equal to the doping charge concentration, P_o. Hence, the total current density $J(t)$ is given by:

$$J(t) = P_o \cdot \upsilon_o(t) + \varepsilon \cdot dE_o(t)/d(t) \tag{2}$$

The first term of the above equation represents the conduction current, where $\upsilon_o(t)$ is the drift velocity and the second term represents the displacement current, where ε is the permittivity of GaAs. Finally, the magnitude of the domain potential at any instant (t) can be given as [14]:

$$\Delta V(t) = \int_{-\infty}^{+\infty} \Delta E(x,t)dx = \Delta V(0) \cdot e^{(-t/\tau_d)} \tag{3}$$

where, $\Delta V(0)$ is the magnitude of the initial disturbance potential which was chosen to be equal to 0.025 V, and τ_d is the decay or growth time of the device.

The effect of neutron fluence (φ) on the carrier mobility (μ) and effective carrier concentration (n) have been determined by a number of researchers [15–17]. It is reported that the main degradation parameters representing carrier removal rate (a) and mobility (b) are defined as:

$$a = (1/n_o) \cdot (dn/d\varphi) \tag{4}$$

$$b = \mu_o (d(1/\mu)/d\varphi) \tag{5}$$

where, μ_o and n_o are the preirradiation values of the carrier mobility and carrier concentration, respectively; μ and n are the postirradiation values.

Using these definitions, one can express the neutron-induced carrier removal and mobility changes by:

$$n = n_o \cdot (1 - a \cdot \varphi) \tag{6}$$

$$\mu = \mu_o/(1 + b \cdot \varphi) \tag{7}$$

where the values for the degradation parameters a and b have been determined for n-type epitaxially grown GaAs as [8]:

$$a(cm^2) = 7.2 \times 10^{-4} (n_o)^{-0.77} \tag{8}$$

$$b(cm^2) = 7.8 \times 10^{-6} (n_o)^{-0.64} \tag{9}$$

Fig. 1 shows the average velocity as a function of applied field υ–E curve, plotted at different neutron fluence (φ) values (Fig. 1A), from which the dependence of both the applied field (Fig. 1B) and average velocity (Fig. 1C) were plotted as a function of neutron fluence. It is clear that the average velocity curves have a negative slope over a broad range of intermediate field values, which is a necessary condition for the existence of negative resistance. Finally, empirical equations concerning the obtained data could be deduced as:

$$E = E_i + B1 \cdot (\varphi) \tag{10}$$

$$E = E_i + 0.27407 \cdot (\varphi) \tag{11}$$

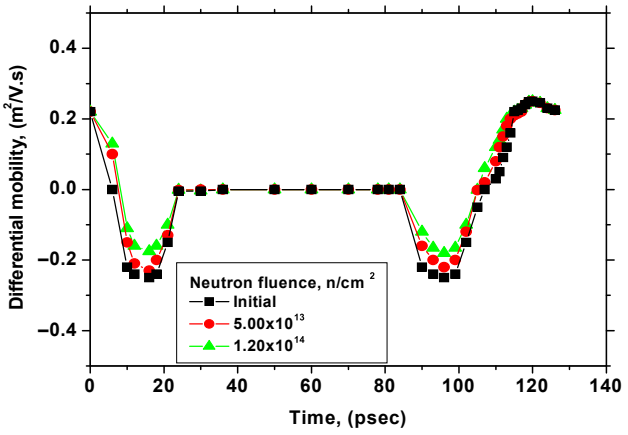

Fig. 3 – Calculated instantaneous change of differential mobility, plotted at different neutron fluences.

$$\upsilon = \upsilon_i + B2\, e^{-(\varphi/t)} \tag{12}$$

$$\upsilon = \upsilon_i + 1.7414\,E15\, e^{-(\varphi/1.33378\ E14)} \tag{13}$$

where E_i: initial value of applied field (E and E_i are given in V/cm); $B1$ and $B2$: constants of the equation and υ_i: initial value of average velocity (υ and υ_i are given in m/s).

The carrier mobility and concentration dependencies on neutron fluence have been calculated applying Eqs. (6 and 7). Both the mobility and concentration of carriers remain uninfluenced with irradiation up to fluence of around 1×10^{12} neutrons/cm^2. For higher neutron fluencies (φ), a sharp decrease was noticed in both cases, as shown in Fig. 2. The following empirical equations could be deduced using the exponential fit:

(a) Carrier mobility (Fig. 2A):

$$\mu = \mu_o + A1 \cdot e^{(-\varphi/t1)} \tag{14}$$

$$\mu = \mu_o + 4,858.0577 \cdot e^{(-\varphi/1.23687\ E14)} \tag{15}$$

where μ and μ_o are given in cm^2/V.s.

(b) Carrier concentration (Fig. 2B and 2C)

$$n = n_o + A1 \cdot e^{(-\varphi/t1)} \tag{16}$$

$$n(10^{20}/cm^3) = n_o(10^{20}/cm^3) + 5.89348 \cdot e^{(-\varphi/2.0839\ E14)} \tag{17}$$

and

$$P = P_o + A1 \cdot e^{(-\varphi/t1)} \tag{18}$$

$$P(10^{20}/cm^3) = 0 + 1.923651 \cdot e^{(-\varphi/6.9657\ E13)} \tag{19}$$

where μ and μ_o: carriers mobility before and after irradiation; p and p_o: holes concentration before and after irradiation; n and n_o: electron concentration before and after irradiation and A1's: constants for each equation.

By differentiating Eq. (1), the differential mobility (μ_d) can be obtained. Fig. 3 shows the change in differential mobility, plotted at different neutron fluences. As the neutron fluence is increased, the mobility begins to be more positive. Up to a fluence level of 1.2×10^{14} neutrons/cm^2, the average mobility becomes nearly positive and thus any existing domain will be decayed.

The domain excess potential was plotted at different neutron fluencies (Fig. 4), applying Eq. (3). By contrast, Fig. 4B shows the dependence of domain excess potential on neutron fluence. The maximum domain excess potential $\Delta V(t)$ is shown to decrease with increasing the neutron fluence and it approximately reaches zero level at a neutron fluence of about 1.20×10^{14} neutrons/cm^2. Finally, empirical equations were deduced as:

$$\Delta V(t) = \Delta V(t)_i - B(\varphi) \tag{20}$$

$$\Delta V(t) = 0.71678 - 0.04752(\varphi) \tag{21}$$

where $\Delta V(t)_i$ is the initial value of domain excess potential, and B is the constant of the equation.

Fig. 5 illustrates the change of the maximum domain excess field (E_d–E_o) and the outside domain field (E_o) with time. As the applied voltage across the diode is increased with time (Fig. 5A), the change of domain excess field (E_d–E_o) was increased up to its maximum value at the instant

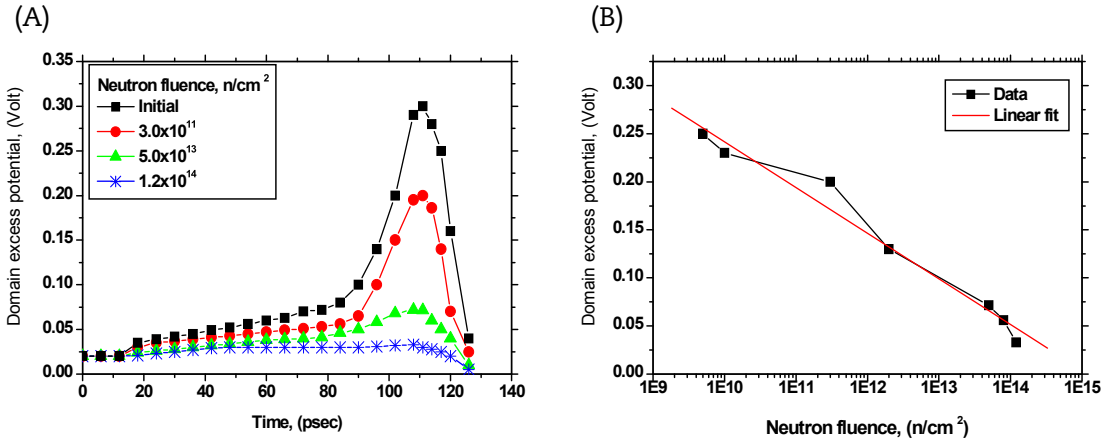

Fig. 4 – (A) Calculated instantaneous change of domain excess potential and (B) domain excess potential plotted at different neutron fluences.

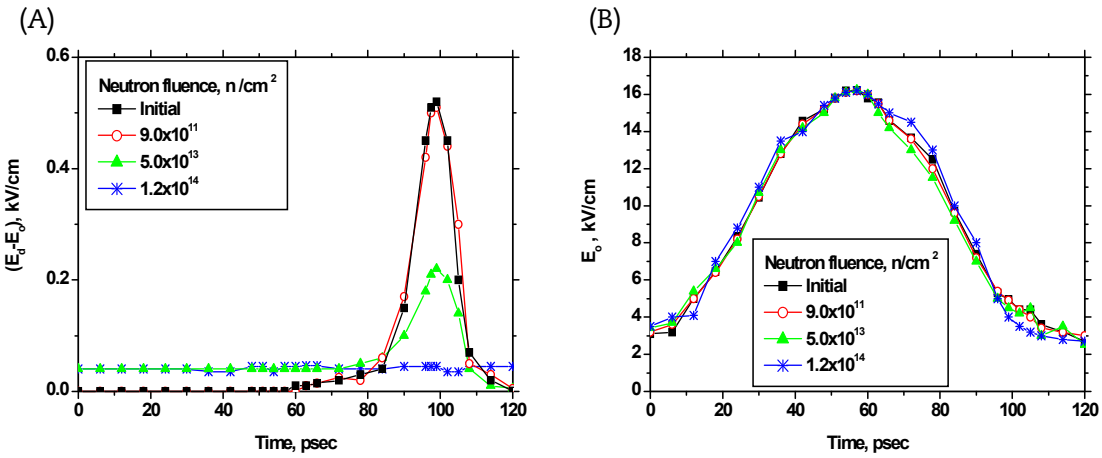

Fig. 5 – Calculated instantaneous change of excess domain field due to neutron exposure.

corresponding to the maximum excess potential (threshold point). After this instant, the domain excess field decreased as $\Delta V(t)$ was decreased. From Fig. 5B, it is clear that the outside domain field (E_o) increased with increasing time up to a certain instant, then decayed with time. Moreover, it is noticeable that E_o is slightly influenced with increasing neutron fluencies. Finally, Fig. 6 shows the dependence of the calculated current density (Eq. 2) on time at two different neuron fluencies (Fig. 6A). The dependence of the current density on different neutron fluencies is shown in Fig. 6B.

$$J(t) = J_o(t) + A1 \cdot e^{(-\varphi/t1)} \tag{22}$$

$$J(t) = J(t)_i + 5.87112 \cdot e^{(-\varphi/1.04725\ E14)} \tag{23}$$

where $J(t)$ and $J(t)_i$ are given in A/mm^2.

The decrease in the current value can mainly be attributed to the fact that the dielectric growth time constant increases due to a decrease in the negative conductivity and the domains do not have time to form before they drift out of the device.

2.2. *Electrical characteristics*

2.2.1. *Choice of devices*

In order to obtain complete data about the effects of radiation on the direct current and microwave characteristics of the TED, its behavior was studied in detail under different operating and irradiation conditions. A commercial fixed frequency CW (continuous wave) GaAs Gunn diode, MA49618 was selected for this experiment, where its electrical characteristics are: V_{Op} = 12 V; I_{Op} = 80 mA; Frequency_{min} = 9.00 GHz; Frequency_{max} = 10.5 GHz; and Power_{min} = 5.0 mW.

2.2.2. *Gamma irradiation*

A γ irradiator, belonging to the National Center for Radiation Research and Technology of Egypt, was used during the course of the present study. It is a Gamma Cell-220, which is a Co-60 irradiator manufactured by Atomic Energy of Canada Limited for use in an unshielded room. As shown in Fig. 7, the unit consists basically of an annular source permanently enclosed within a lead shield, a cylindrical drawer up or down

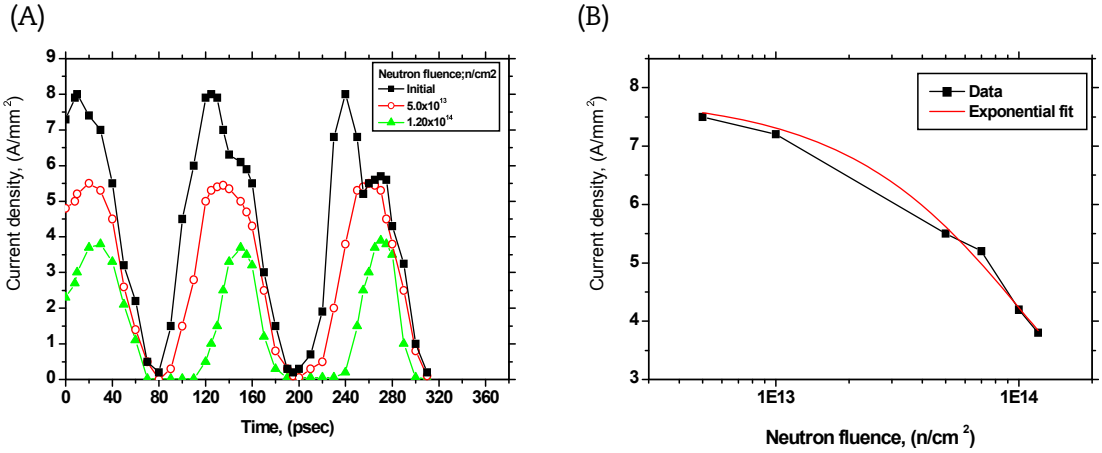

Fig. 6 – Calculated instantaneous change of external current density. Plotted at (A) different neutron fluencies and (B) dependence of current density on neutron fluence.

Fig. 7 – Overall view of Gamma Cell 220.

along the source centerline. The drawer has a chamber for carrying samples to be irradiated from outside. Samples up to approximately 15 cm in diameter and 20 cm in height can be accommodated in the chamber. An electrically powered digital timer automatically raises the drawer at the termination of a sample irradiator. Time can be preset either automatically to a maximum of 999.9 hours or to a manual operation position. Finally, the samples were irradiated with ascending gamma-doses of up to 12 kGy, at a rate of 0.35 Gy/s. Reference dosimeters were always applied for irradiation quality control adjustment.

2.3. *Annealing of radiation damage*

The annealing of radiation damages in semiconductor devices usually follows one of three different approaches: rapid annealing; slow annealing; or thermal annealing [18]. Rapid annealing is usually performed at high temperature where it takes little time for the device to recover. Slow annealing proceeds at room temperature. By contrast, thermal annealing implies elevated temperatures. Other types of annealing are also possible where the device may be subjected to a symmetrical high-frequency electromagnetic field or bias temperature stressing.

2.3.1. *Self/shelf annealing*

Irradiated samples were left on a shelf, at room temperature, while plotting their electrical characteristics periodically. Measurements were carried out up to the recovery saturation conditions, where no more annealing effect was noticed.

2.3.2. *Isochronal/oven annealing*

The temperature of the irradiated sample has been raised up to different levels (to 60°C, 80°C, and 100°C) for different annealing times (0.5 hours, 1.0 hours, 1.50 hours, 2.0 hours, 2.5 hours, 3.0 hours, 3.5 hours, and 4.0 hours). For each annealing time step, the sample was left to cool down to room temperature. Its electrical characteristics were then measured.

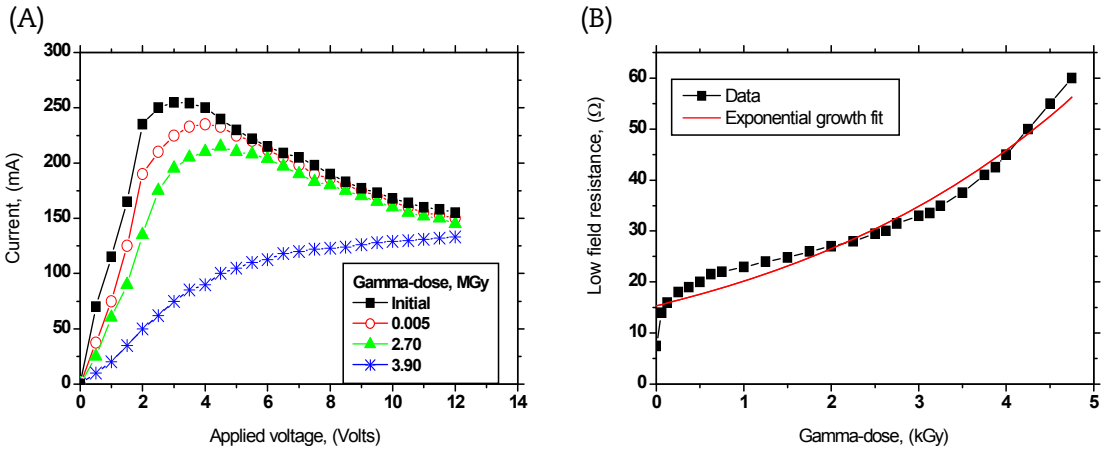

Fig. 8 – (I–V) characteristic curves for GaAs Gunn diodes. (A) Plotted under the influence of different γ dose levels and (B) the dependence of low-field resistance on γ dose.

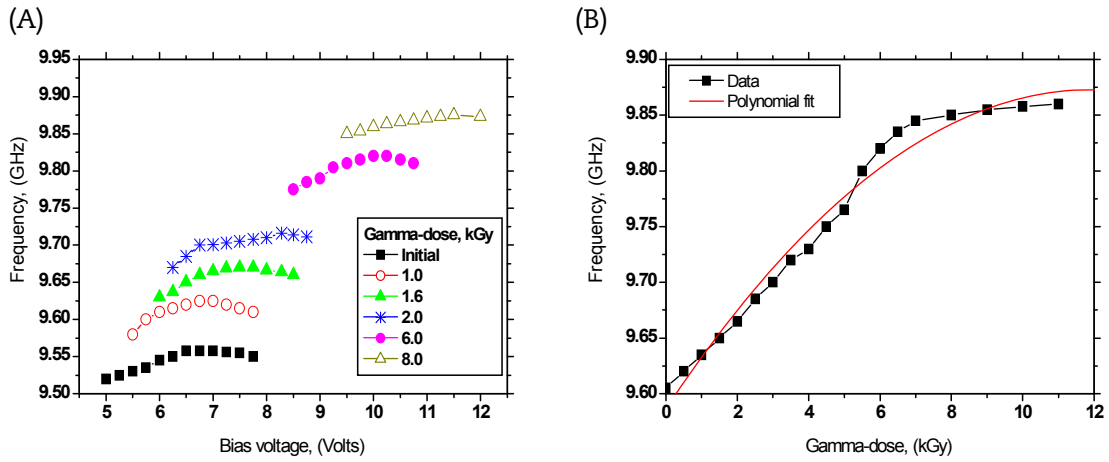

Fig. 9 – Dependence of operation frequency of Gunn diode oscillator bias voltage. (A) Plotted at different γ dose levels and (B) dependence of oscillation frequency on γ dose.

3. Results and discussion

3.1. *Direct current characteristics*

During the present part of the work, the (I–V) characteristic curves of the investigated Gunn devices were plotted before and after exposure to ascending γ dose levels. The state of the 370A curve tracer, manufactured by Tektronix, which is a high-performance, general purpose interface bus-programmable digital-storage instrument, can provide static and dynamic semiconductor device characteristics measurement. The instrument stimulates, measures, and displays the semiconductor characteristics of a variety of two- and four-terminal devices. Fig. 8A shows the γ irradiation effects on the (I–V) characteristics of Gunn devices (TEDs). It is clear that there are two important regions of interest in each curve. The first is below the threshold voltage (approx. 3.5 V), where the low field resistance (R_o) is shown to increase with irradiation (Fig. 8B). The matter that is mainly attributed to the decrease in both initial carrier concentration (n_o) and carrier mobility (μ_1) with γ exposure is due to the carrier removal effect, and:

$$R_o = L/n_o \cdot q \cdot \mu_1 \cdot A \tag{24}$$

where R_o: low-field resistance and L and A: length and cross-sectional area of the device, respectively.

Concerning the dependence of the low field resistance on the gamma-irradiation dose, an exponential relationship was obtained, where:

$$R_o = R_{oi} + A \cdot e^{(-x/t)} \tag{25}$$

$$R_o = 0 + 15.35145 \cdot e^{(-\varphi/3.65809)} \tag{26}$$

The second region of interest is observed at voltage values above threshold levels (>3.5 V), and for γ-doses below 3.90 MGy where negative resistance changes are mainly due to domain formation. Finally, for γ-doses above 3.90 MGy, the devices lose their main feature as negative resistance devices and behave as linear positive resistance devices.

3.2. *Microwave characteristics*

3.2.1. *Oscillation frequency*

During the course of the study, frequency characteristics of the Gunn diode for a millimeter wave oscillator were investigated [19–21]. The dependence of the operating frequency (F_{op}) on the bias voltage is shown in Fig. 9A. It is clear that the frequency is a direct function of the γ exposure (γ) and it increases in a linear manner up to a total dose of 8.0 kGy (Fig. 9B). For higher γ doses, the effect was shown to be insignificant, which means that the radiation damage reaches saturation level. The obtained dependence of the oscillation frequency on γ dose could be expressed in the manner shown in the following equation, where the polynomial fit could be expressed as:

$$F_{op} = F_{opi} + B_1 \cdot x + B_2 \cdot x^2 \tag{27}$$

$$Frequency = 9.58686 + 0.04804 \cdot (\gamma) + (-0.00202) \cdot (\gamma)^2 \tag{28}$$

The observed increase in frequency can be explained in the presence of the simplified equivalent circuit diagram of the Gunn diode oscillator (Fig. 10). The cavity parameters are represented by L, C, and R_L, while that for the diode is represented by $-R_n$ (most of C is due to device capacitance). The operating frequency is determined by both the cavity and L/R time constant, hence:

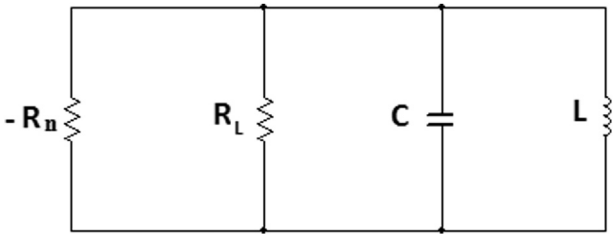

Fig. 10 – Simplified equivalent circuit of a relaxation mode Gunn diode oscillator.

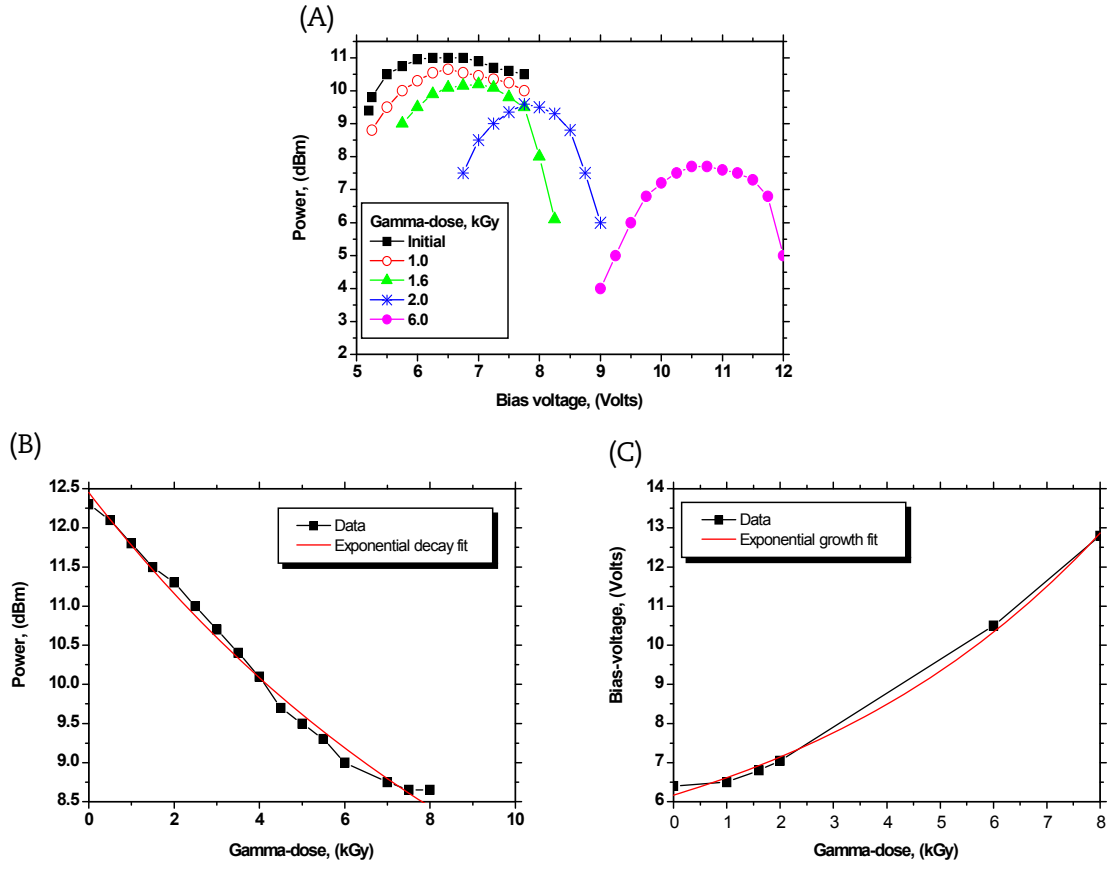

Fig. 11 – Dependence of output power of Gunn diode oscillator on bias voltage. (A) Plotted at different γ dose levels, and dependence of (B) output power and (C) bias voltage on γ dose.

$$T = 1/F_{op} = 2\pi\sqrt{LC} + L/R_o \cdot M \tag{29}$$

where, M is the bias/threshold voltage ratio ($= E_B/E_T$).

Now, referring to the previously stated relationships for the radiation effects on the low field resistance and the ratio M, it is clear that both R_o and M are increased by γ exposure. As a result, and from Eq. (29), it is clear that a decrease in the time constant (T) occurs as a function of the increases in R_o and M. Therefore, a corresponding increase will appear in the oscillation frequency.

3.2.2. *Effects on radio frequency output power*

The dependence of the radio frequency oscillator output power on the bias voltage was plotted under the influence of different γ-dose levels (Fig. 11A). The power increased with bias voltage reached a peak value and then decreased slowly with increasing the bias voltage. As the devices are exposed to γ radiation, severe interruption occurs to their power characteristics. The maximum peak output power was decreased (Fig. 11B), while the bias is shown to be shifted toward higher voltage values (Fig. 11C), resulting in an increase in the bias/threshold voltages ratio. Finally, the dependence of output power on γ dose was plotted where an empirical equation was deduced as:

$$P_{out} = P_{outi} + A \cdot e^{(-x/t)} \tag{30}$$

$$Power = 4.672 + 7.7813 \cdot e^{(\gamma(kGy)/11.02261)} \tag{31}$$

$$V_B = V_{Bi} + A \cdot e^{(x/t)} \tag{32}$$

$$V_B = 3.54799 + 2.61778 \cdot e^{(\gamma(kGy)/6.29982)} \tag{33}$$

where P_{out} and P_{outi}: output power before and after γ irradiation are given in (dBm); V_B and V_{Bi}: bias voltage before and after γ irradiation (given in V) and A and B: constants of the equation.

The decrease in maximum peak output power can be understood from an inspection of the previously mentioned equivalent circuit (Fig. 10). The condition for oscillation requires that $|R_n| < R_L$, and the fall off in power before failure is reached due to the following:

i. Since these devices are operated at a constant voltage, the decrease in operating current that occurs with increased resistance results in a reduced output power, and
ii. For $n \cdot L$ products below the optimum value, the efficiency is decreased as $n \cdot L$ is decreased. An upper limit on output occurs due to the fact that $|R_n|$ is increased with bias. This

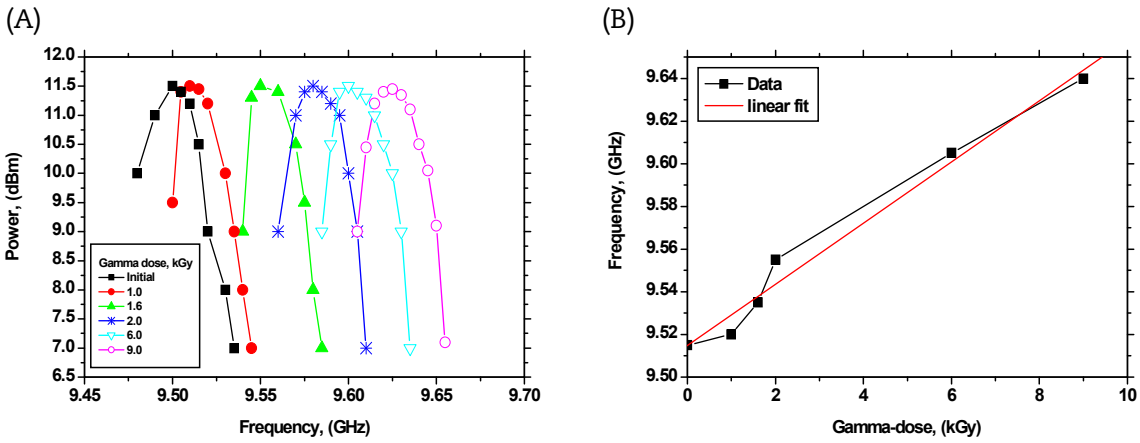

Fig. 12 – Dependence of output power of Gunn diode oscillator on frequency. (A) Plotted at different γ dose levels, and (B) dependence of frequency on γ dose.

can be demonstrated as follows: near breakdown, $|R_n|$ has the form:

$$|R_n| = K \cdot R_o \cdot M \tag{34}$$

where, K is constant for large values of M.

Therefore, it can be seen that as E_B is increased, M is increased, and if $|R_o| > R_L$, oscillation will cease and breakdown can occur. Therefore, it can be seen from Eq. (34) that as R_o is increased, with irradiation, the maximum allowable value of M will be decreased if the condition that $|R_o| < R_L$ is to be satisfied. This in turn means that the maximum peak power output is decreased, since the allowable bias voltage must be reduced.

It is clearly shown in Fig. 12A that as the γ-dose is increased, the same maximum power is caused at higher frequency, which can be understood from Eq. (35), since this means that by increasing the γ-dose, T will be decreased and, so, the frequency of oscillation will be increased. While for the same dose, it is observed that the power will be decreased from the maximum value, due to the effect of the loading circuit. Finally, Fig. 12B shows the dependence of the oscillation frequency on γ dose, where:

$$F_{osc} = F_{osci} + B \cdot (\gamma) \tag{35}$$

$$F_{osc} = 9.51486 + 1.433E - 2(\gamma; kGy) \tag{36}$$

where, F_{osci}: is the initial oscillation frequency of the oscillator, and B: constant of the equation.

3.3. *Annealing of radiation damage*

To ascertain the behavior of the irradiated Gunn devices, their electrical characteristics were plotted under two annealing methods.

3.3.1. *Self/shelf annealing*

Primarily, self/shelf annealing is a technique in which the irradiated devices were left at air temperature (room level) and so may be cold-worked without strain-hardening. In this respect, the electrical characteristics of the irradiated samples, which were kept at room temperature, were tested weekly, where the (I–V) characteristic curves of Gunn diode, plotted after irradiation and different shelf annealing periods are shown in Fig. 13A. Fig. 13B shows the recovery percentage of the Gunn devices plotted as a function of self-annealing time, following Eq. (37). From this it is clearly noticed that for annealing times of more than around 12 weeks, the rate of annealing was negligible, i.e., the saturation condition was almost reached.

$$Y = Y_o + A \cdot e^{(-x/t)} \tag{37}$$

$$Y = 0.80386 + (-0.27787) \cdot e^{-(time;weeks)/1.99966} \tag{38}$$

where, Y_o: is the ratio of the device current after to before irradiation, and A: constant of the equation.

3.3.2. *Isochronal/oven annealing*

The temperature of the irradiated devices has been raised up to 60°C, 80°C, and 100°C for different annealing times of 0.5 hours, 1.0 hours, 1.5 hours, 2.0 hours, 2.5 hours, 3.0 hours, 3.5 hours, and 4.0 hours, then each of the samples were left until room temperature was reached. The obtained data show that for the investigated three annealing temperature levels, the maximum recovery percentages of 70%, 81%, and 91.5% were reported. Note that no more heat could be applied due to the temperature operating range of the devices under test. Finally, the recovery percentage of the irradiated devices, under the influence of 100°C, as an example, was plotted as shown in Fig. 13C, following the empirical equation:

$$Y = Y_o + B_1 \cdot x + B_2 \cdot x^2 \tag{39}$$

$$Y = 0.49931 + 0.24109 \cdot (annealing\ time,\ hr.) + (-0.03455) \cdot (annealing\ time,\ hr.)^2 \tag{40}$$

4. Conclusion

The performance of a Gunn diode for a microwave oscillator under the influence of neutron and γ fields was investigated. To this end, different empirical equations were deduced,

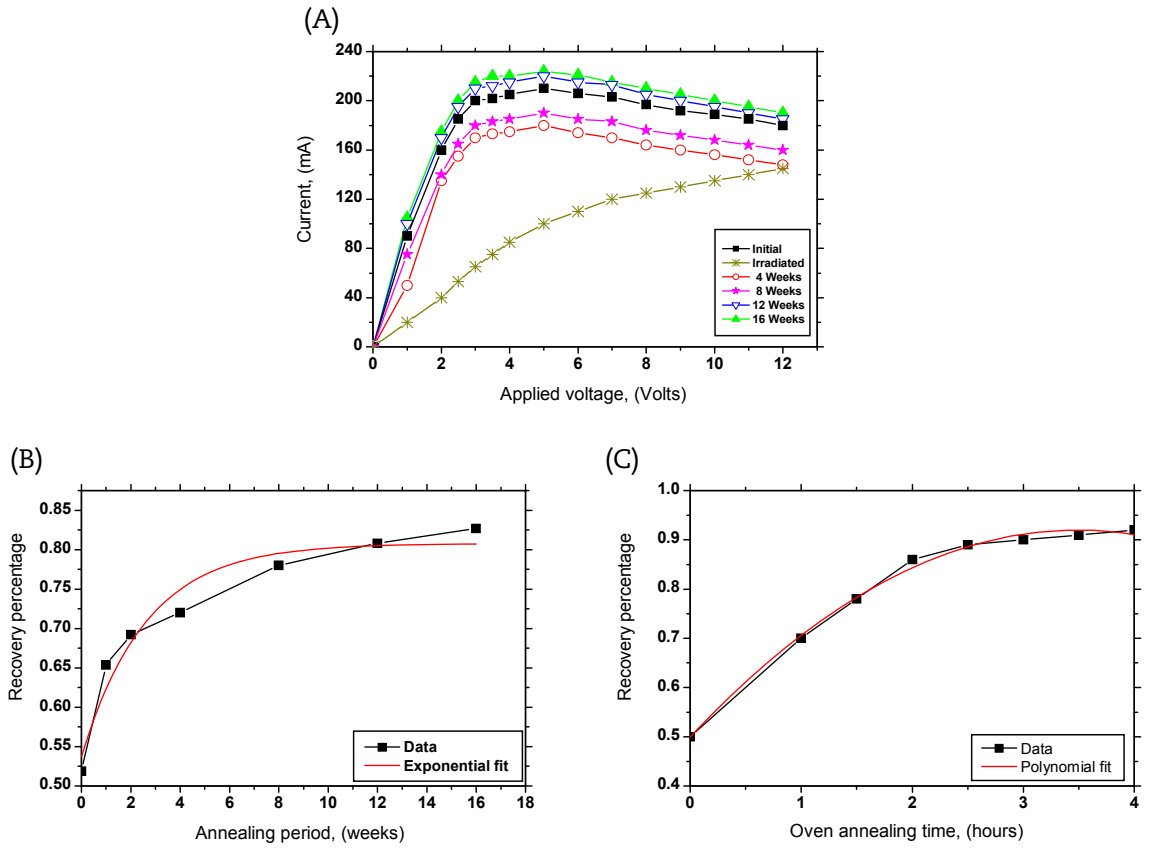

Fig. 13 – (I–V) characteristic curves of Gunn diode. (A) Plotted after irradiation and different shelf annealing periods, recovery percentages a function of (B) annealing period and (C) oven annealing time at 100°C.

tested, and proved to be satisfactory in representing the behavior of a Gunn diode and its oscillation circuit. It was shown that radiation influences the Gunn diode oscillator operation; the matter is mainly due to the reduction of carrier mobility, as a result of the introduced traps and reduction in the effective carrier concentration. As a result, the radiation causes the oscillation frequency to increase and the output power and bias current to decrease. Higher γ dose levels cause the devices to lose their main feature as negative resistance devices and behave as a linear positive resistance device. Finally, oven and self-annealing processes were to shown to be acceptable techniques for devices to recover to their complete initial characteristics.

Conflicts of interest

The authors declare no conflicts of interest.

REFERENCES

[1] K.G. Naik, S. Bhat, G. Sangeev, The effect of electron irradiation on BJTs and MOSFETs at elevated temperatures, Arch. Phys. Res. 4 (2013) 74–86.
[2] D. Nikolić, A. Vasić, I. Fetahović, K. Stanković, P. Osmokrović, Photodiode behavior in radiation environment, Sci. Publ. State Univ. Novi Pazar Ser. A: Appl. Math. Inform. Mech. 3 (2011) 27–34.
[3] M. Zdravkovic, A. Vasic, B. Cavric, R. Radosavljevic, K. Stankovic, Radiation induced noise level in solar cells, in: PIERS Proceedings, Kuala Lumpur, Malaysia, March 27–30, 2012, pp. 1160–1164.
[4] R. Katz, K. LaBel, J.J. Wang, B. Cronquist, R. Koga, S. Penzin, G. Swift, Radiation effects on current field programmable technologies, Nucl. Sci. IEEE Trans. 44 (1997) 1945–1956.
[5] Z. Pavlović, I. Manić, S. Golubović, Effects of γ-irradiation on electrical characteristics of power VDMOS transistors, Facta Univ. Ser. Phys. Chem. Technol. 2 (2002) 223–233.
[6] A. Förster, J. Stock, S. Montanari, M.I. Lepsa, H. Lüth, Fabrication and characterisation of GaAs Gunn diode chips for applications at 77 GHz in automotive industry, Sensors 6 (2006) 350–360.
[7] S.I. Domrachev, S.A. Alaverdjan, V.N. Skorokhodov, Application of a Gunn-diode current-pulse generator for modulation of semiconductor lasers, Tech. Phys. 44 (1999) 544–547.
[8] H.W. Thim, Computer study of bulk GaAs devices with random one-dimensional doping fluctuations, J. Appl. Phys. 39 (1968) 3897–3904.
[9] K.K. Thornber, Current equations for velocity overshoot, IEEE Electron Device Lett. EDL-3 (1982) 69–71.
[10] T. Wang, K. Hess, Calculation of the electron velocity distribution in high electron mobility transistors using an ensemble Monte Carlo method, J. Appl. Phys. 57 (1985) 5336–5339.
[11] N. Berg, H. Dropkin, Neutron displacement effects in epitaxial Gunn diodes, IEEE Trans. Nucl. 17 (2007) 233–238.

[12] G.E. Brehm, G.L. Pearson, Effects of gamma radiation on Gunn diodes, IEEE Trans. Electron Devices 17 (2005) 475–479.
[13] D.J. Widiger, C. Kizilyalli, K. Hess, J.J. Coleman, Two-dimensional transient simulation of an idealized high electron mobility transistor, IEEE Trans. Electron. Devices. ED-32 (1985) 1092–1102.
[14] P.J. Price, On the flow equation in device simulation, J. Appl. Phys. 63 (1988) 4718–4722.
[15] I.C. Kizilyalli, K. Hess, Simplified device equations and transport coefficients for GaAs device modeling, IEEE Trans. Electron Devices 34 (1987) 2352–2354.
[16] R.K. Parida, N.C. Agrawala, G.N. Dash, A.K. Panda, Characteristics of a GaN-based Gunn diode for THz signal generation, J. Semiconductor 33 (2012) 084001–084007.
[17] V. Eremin, Z. Li, Carrier drift mobility study in neutron irradiated high purity silicon, Nucl. Instr. Meth. Phys. Res. A: Accelerators Spectrometers Detectors Assoc. Equip 362 (1995) 338–343.
[18] M.I. Gorlov, D.A. Litvinenko, Annealing of radiation and electrostatic damages in semiconductor devices, Russian Microelectronics 31 (2002) 295–304.
[19] L.B. Lin, Z.J. Liao, Q. Liu, T.C. Lu, X.D. Feng, Effect of proton irradiation on electric properties in AlGaAs/GaAs heterostructure materials, Surface and Coatings Technology 158–159 (2002) 737–740.
[20] J. Huang, H. Yang, C. Tian, J.R. Dong, H.Y. Zhang, T.Y. Guo, Design and manufacture of planar GaAs Gunn diode for millimeter wave application, Chin. Phys. B 19 (12) (2010) 127203-1–127203-5.
[21] Z. Greenwald, D.W. Woodard, A.R. Calawa, L.F. Eastman, The effect of a high energy injection on the performance of mm wave Gunn oscillators, Solid-State Electronics 31 (1988) 1211–1214.